Journal of the Korean Ceramic Society
Vol. 43, No. 11, pp. 680~687, 2006.

Review

Smart Solid State Syntheses of Well-Crystallized Phase Pure Mixed Oxides for Electroceramics

Mamoru Senna†

Faculty of Science and Technology, Keio University, Yokohama 223-8522, Japan
(Received October 19, 2006; Accepted October 31, 2006)

ABSTRACT

An overview is given to optimize the solid state processes toward phase pure and well-crystallized fine particulates of mixed oxides, serving as electroceramic materials in various genres. Elevation of the reactivity and preservation of stoichiometry of the starting mixture are of universal importance. Mechanical activation is versatile for these purposes, particularly when an oxygen atom as a hinge promotes formation of hetero-bridging bonds between dissimilar cationic species prior to calcination. Case studies carried out recently in the author's laboratory are displayed and compared for ferroelectric materials, *i.e.* $PbMg_{1/3}Nb_{2/3}O_3 \cdot xPbTiO_3$ (PMN-PT), $(1\text{-}y)Pb(Zn_xMg_{1-x})_{1/3} \cdot yNb_{2/3}O_3$ (PZN-PMN), $BaBi_2Ta_2O_9$ (BBT), $Ba(Mg_{1/3}Ta_{2/3})O_3$ (BMT), and ferromagnetics, *i.e.* M-, Y-, and Z-phases of Ba-hexaferrites.

Key words **: *Electroceramic materials, Soft-mechanochemical synthesis, Solid state processes, Reactivity of solids, Mixed oxides***

1. Introduction

In the last three decades, where Professor Sang Hee Cho was active in Kyungpook National University, technology around electroceramics seems to have made one closed cycle of its development. The cycle was started from the improvement of a solid state processes, as he himself fought with his own dissertation for Ph.D degree. Immediately thereafter, a boom exploded for non-ceramic processes including sol-gel or solution processes, chemical and physical deposition or hydrothermal routes. All these then-novel processes look wonderful and indeed many of them are quite successful.

With the turnaround of the millennium, however, ceramic processes came under spotlight and reevaluated. The reason for this turn is quite manifold. Increased awareness of environmental benign and cost conscious favor processes with smaller amount of solvents, lower processing temperature, in short, under conditions as close to the ambient one as possible. This inevitably requires increase in the reactivity of solids.

Solid state processes are indeed more advantageous than competing alternatives *via* solution of vapor phases to fabricate electroceramic materials due primarily to high productivity, cost merits and echology. For a solid-state process or a ceramic process have to overcome well known shortcomings of inhomogeneity, low reactivity and associated necessity of high temperature often leading to disfavored grain growth. Well-dispersed, fine particulate raw materials are commercially available at a reasonable price nowadays, so that the main purpose of milling a mixture is shifted from size reduction to homogenization of the reaction mixture. Appropriate choice of the starting species of cationic ingredients may not be underestimated either.

To obtain a homogeneous powder mixture, ball mills are used routinely, mostly, in alcohol. Related to the demands for nanoparticles, various mills appeared to give highest possible energy density. This does not match the present purpose. High intensity milling is quite often hazardous, due chiefly to serious contamination and stoichiometry loss. It is therefore very important to exert mechanical stress as sparingly as possible by knowing what is absolutely beneficial by virtue of mechanical stressing. Importance and charm of the mechanical stressing under the concept, coined as soft-mechanochemical processing, are established.[1-10]

Optimal condition of starting mixtures, including appropriate choice of the starting species of cationic ingredients and possible merits of additives will be demonstrated below, based on the case studies carried out recently in the author's laboratory for ferroelectric materials, *i.e.* $PbMg_{1/3}Nb_{2/3}O_3 \cdot xPbTiO_3$ (PMN-PT), $(1\text{-}y)Pb(Zn_xMg_{1-x})_{1/3} \cdot yNb_{2/3}O_3$ (PZN-PMN), $BaBi_2Ta_2O_9$ (BBT), $Ba(Mg_{1/3}Ta_{2/3})O_3$ (BMT), and ferromagnetics, *i.e.* M-, Y, and Z-phases of Ba-hexa-ferrites.

2. PMN-PT

In our case study on the complex perovskite, $PbMg_{1/3}Nb_{2/3}O_3$ (PMN) with and without coexistence of $PbTiO_3$ (PMN-xPT with x=0, 0.1 or 0.2),[11] we started from a stoichiometric mixture comprising respective oxides with an exception of $Mg(OH)_2$, being a stable hydroxide, instead of MgO. As

†Corresponding author : Mamoru Senna
E-mail : senna@applc.keio.ac.jp
Tel : 81-45-566-1569 Fax : 81-45-564-0950

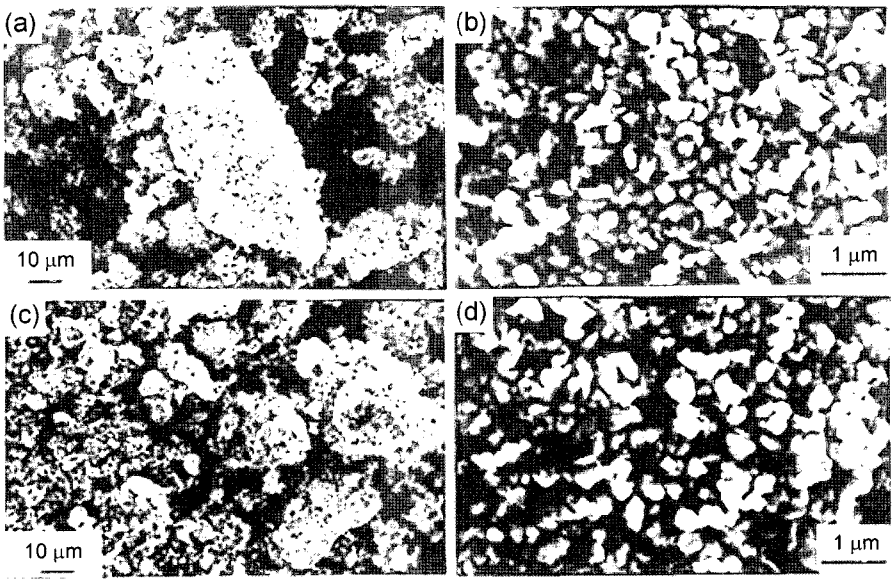

Fig. 1. Scanning electron micrographs of the reaction mixture for PMN-xPT: Left and right columns; before and after mechanical homogenization, respectively. (a) and (b): $x=0$; (c) and (d): $x=0.1$.

shown in Fig. 1, degree of agglomeration of the starting mixture substantially decreases after milling with a multi-ring mill[12] for 60 min. While total deagglomeration by powder processing is generally not possible, size distribution of the aggromerates always narrows toward homogenization in 100 nm regime. Homogeneity in the nanometer regime was also quantified by using the standard deviation of the local atomic ratio from the overall nominal one determined by EDX installed in the transmission electron microscope.[11]

It is, however, more important to notice that the mixture is chemically homogenized as well. As shown in Fig. 2, oxygen 1s XPS spectra changes from the multimodal one reflecting those of individual starting materials to that of the solid solution, i.e. the end product. The increase in the relative intensity of Pb-O-multi component B-site ions by mechanical treatment is attributed to the formation of new chemical bonds as a result of chemical interactions between dissimilar components.

As we calcined the mechanically homogenized mixtures mentioned in the previous section at 850°C for 4 h, we obtained always phase pure perovskite, as shown in Fig. 3.[11] Morphology of the calcined powders is also much more uni-

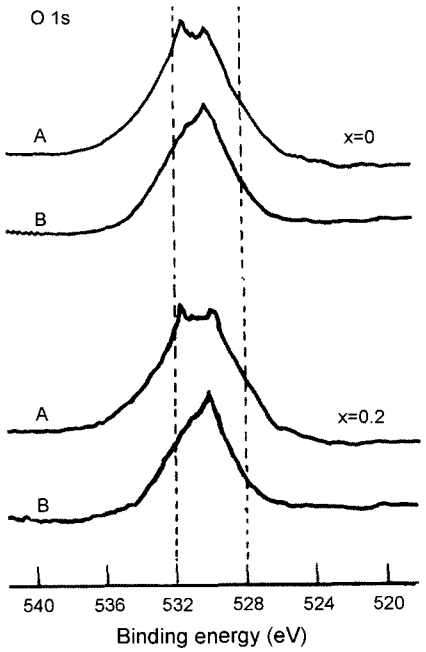

Fig. 2. X-ray photoelectron spectra of the reaction mixture for PMN-xPT. T0, T10, and T20 denote, $x=0$, 0.1, and 0.2, respectively. Extention –60 denotes mechanically milled for 60 min.

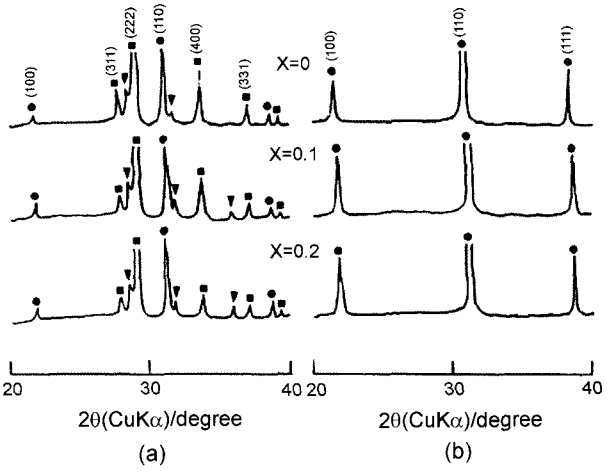

Fig. 3. X-ray diffraction profiles of PMN-xPT after firing at 850°C for 4 h. Columns (a) and (b) correspond to the starting materials without and with mechanical homogenization, respectively.

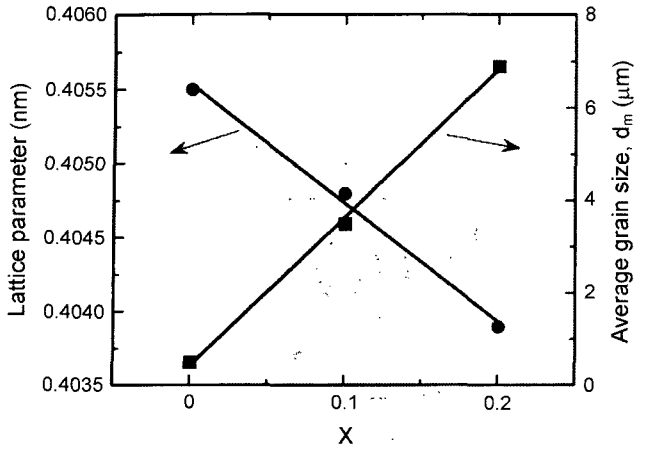

Fig. 4. Lattice parameter, a, and average grains size of PMN-xPT after firing at 850°C for 4 h.

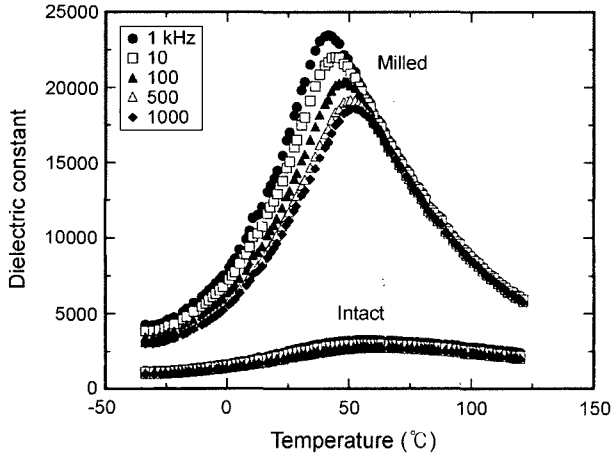

Fig. 5. Frequency dependence of the dielectric constant of PMN-0.1PT after sintering at 1200°C for 2 h. Extension –60 denotes homogenized for 60 min.

form when we started from homogenized mixture. The lattice constant decreased linearly with x, as shown in Fig. 4, indicating the formation of uniform PMN-PT solid solution. As expected, dielectric properties exhibit large differences, with typical characteristics of the relaxer in the case of starting from the homogenized mixture, as shown in Fig. 5. The obvious superiority of the mechanically pretreated products is primarily attributed to the elimination of the second phase, pyrochlore.

3. PMN-PZN

Even more difficult than PMN is to synthesize PZN, where Mg in PMN is substituted by Zn. Difficulty is chiefly attributed to the thermodynamic instability of PZN, so that we expect kinetic stabilization to arrive at the crystalline state as rapidly as possible and to quench before decomposition or further phase transformation takes place. Since the hurdle for pure PZN was too high, we tried to prepare PZN-PMN solid solution with minimum possible portion of PMN.

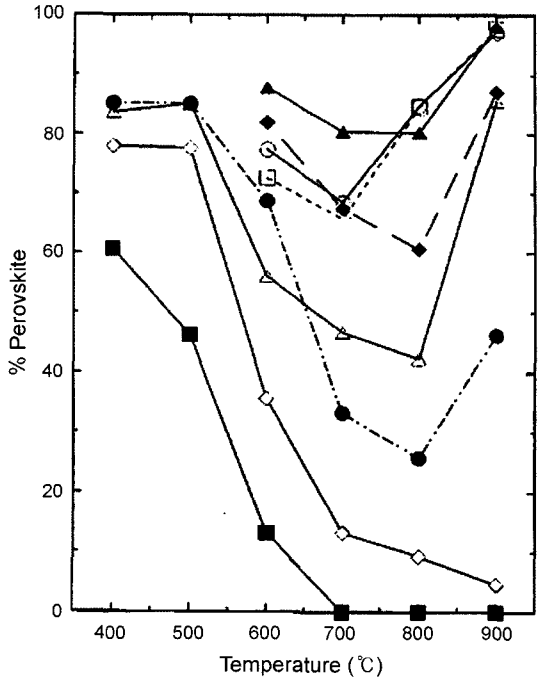

Fig. 6. Plots of percent perovskite against firing temperature for mixtures milled for 180 min. Different curves corresponding different x varying from top to bottom: 0 (PMN), 0.2, 0.4, 0.6, 0.7, 0.8, 0.9, and 1.0 (PZN).

We first mixed PbO, $Mg(OH)_2$, Nb_2O_5 and $2ZnCO_3 \cdot 3Zn(OH)_2 \cdot H_2O$ in a desired stoichiometry.[13] A compound $2ZnCO_3 \cdot 3Zn(OH)_2 \cdot H_2O$ possesses higher basicity than any other commercially available Zn salts in a powdery form.

It is to be emphasized that a set of new XRD peaks corresponding to perovskite appear from early stages of milling. Relative intensity of perovskite peaks increases with milling time. On subsequent heating up to 400°C and quenching, perovskite became a sole crystalline phase. As shown in Fig. 6, percent perovskite decreases and again increases after showing a minimum at temperatures 700~800°C for the mixtures up to x=0.8. We attributed the increase in the perovskite to the incorporation of PMN into PZN due to restabilization of the perovskite phase. No recovery of perovskite is observed for the components with x=0.9 and x=1.0 (pure PZN).

It has been theoretically calculated that substitution of Pb(II) at A-site by Ba up to 10 mol% or Zn at B-site by Mg up to 7.4 mol% will stabilize PZN.[14,15] In actual fact, however, additive concentration as high as 40 mol% Mg to PZN ($PZ_xM_{1-x}N$ with x=0.6) was necessary for phase pure perovskite.[16] Instability of perovskite $PZ_xM_{1-x}N$ is thus much higher than theoretically expected. Rapid formation of a $PZ_xM_{1-x}N$ solid solution at relatively low temperatures, where lattice strain is still accommodated to tolerate the perovskite structure, is the essence of the successful synthesis. As a matter of fact, continuous increase in the X-ray diffraction peak breadth of perovskite was observed with increasing the fraction of PZN, x, as shown in Fig. 7.

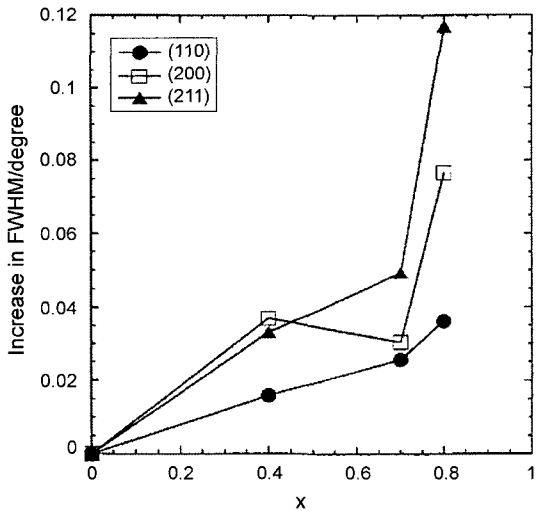

Fig. 7. Increase in the full-width at half-maximum of XRD peaks with fraction of PZN, x, for mixtures milled for 180 min and fired at 1100°C for 1 h.

4. $BaBi_2Ta_2O_9$ (BBT) and $Ba(Mg_{1/3}Ta_{2/3})O_3$ (BMT)

We have applied soft-mechanochemical processes to synthesize lead-free electroceramics as well. $BaBi_2Ta_2O_9$ (BBT) and $Ba(Mg_{1/3}Ta_{2/3})O_3$ (BMT), particularly useful for microwave dielectrics.[17,18] We started from Bi_2O_3 and Ta_2O_5 as starting materials. The stoichiometric mixture was milled with nylon balls in vibratory mill for 3 h and was calcined for 1 h in air at temperatures between 850 and 1000°C. For BMT, $BaCO_3$, and $Mg(OH)_2$ were used as Ba and Mg sources and either Ta_2O_5 or $Ta_2O_5 \cdot 3.8H_2O$ was used as Ta source. $Ta_2O_5 \cdot 3.8H_2O$ was prepared from ethanol solution of $TaCl_5$ by adding NH_3 aqueous solution. The molar amount of hydrated water per mole of Ta_2O_5 was determined to be 3.8 by thermogravimetry.

Fully crystallized, fine particulate BBT was obtained by firing the mechanically activated starting mixture at 900°C, when we started from $BaCO_3$, Bi_2O_3, and Ta_2O_5. The resultant particles are rather uniform with their average grain size as small as 600 nm, as shown in Fig. 8.

In the case of $Ba(Mg_{1/3}Ta_{2/3})O_3$ (BMT), in contrast, similar success was only reached by using hydrated sample, $Ta_2O_5 \cdot 3.8H_2O$, in place of anhydrous Ta_2O_5. As shown in Fig. 9, the second phase, $BaTi_2O_4$, was almost disappeared, if not completely, by using mechanically activated mixture with $Ta_2O_5 \cdot 3.8H_2O$, as shown in Fig. 9(b). Note that the remarkable effect of milling is obvious here, again, by comparing the calcined products starting from the intact mix-

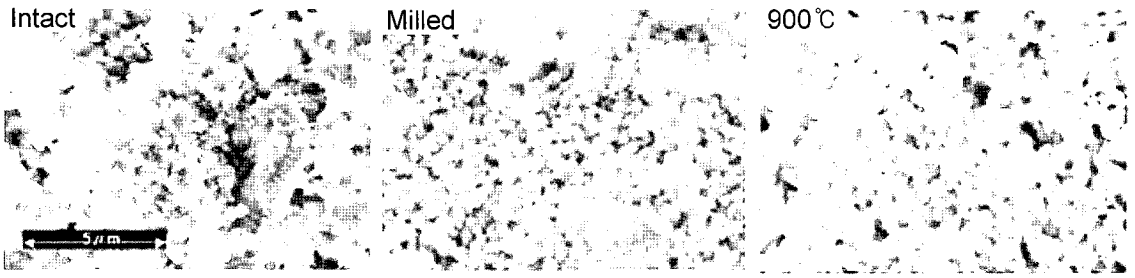

Fig. 8. Scanning electron micrographs of the starting mixture without milling (intact), milled by a laboratory sized vibration mill for 3 h (milled) and subsequently calcined at 900°C for 1 h.

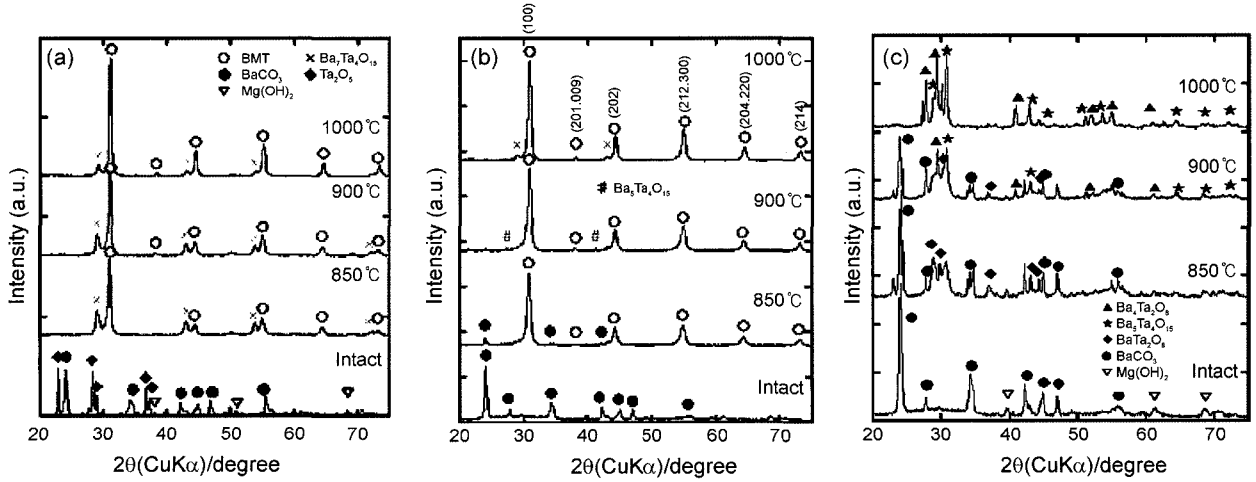

Fig. 9. X-ray powder diffractograms for BMT calcined at varying temperatures derived from the mixtures containing (a) Ta_2O_5, milled for 3 h, (b) $Ta_2O_5 \cdot 3.8H_2O$ milled for 3 h, and (c) (b) $Ta_2O_5 \cdot 3.8H_2O$ without milling.

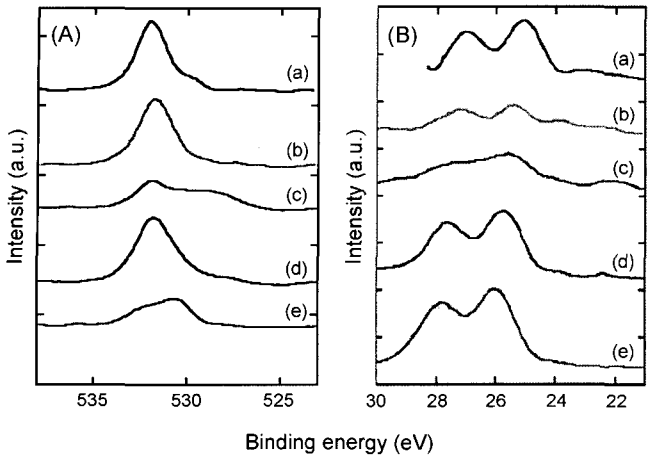

Fig. 10. XPS profiles of (A) O1s and (B) Ta4f. For each profiles, assignment of the curves are: (a) oxide mixture, (b) milled sample (a), (c) hydrated oxide mixture, (d) milled (c), and (e) fired sample (d).

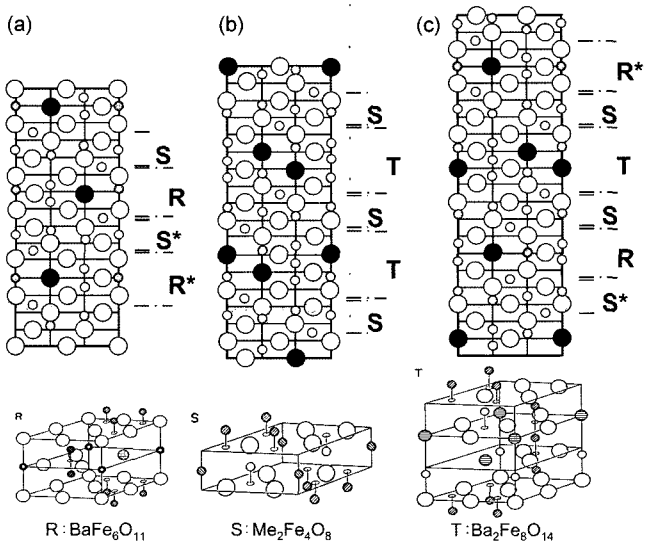

Fig. 11. Layer structures of (a) M-phase, (b) Y-phase, and (c) Z-phase.

ture with $Ta_2O_5 \cdot 3.8H_2O$, as shown in Fig. 9(c).

In Fig. 10(a), O1s XPS profiles are displayed for (a) Ta_2O_5-derived mixture, (b) sample (a) after milling for 3 h, (c) $Ta_2O_5 \cdot 3.8H_2O$-derived mixture, (d) sample (c) after milling for 3 h, and (e) BMT obtained by calcining sample (d) at 900°C, respectively. A second peak appeared in curves (c) at the lower binding energy is ascribed to the hydrated water aid is disappeared after milling. We attributed this to the consumption of hydrated water due to the formation of bridging bonds, Ba-O-Ta and Mg-O-Ta across the boundary of dissimilar particle species. As for the binding energy of Ta4f, it is particularly noteworthy by referring Fig. 10(B), where curves (a)~(e) correspond to those of Fig. 10(A), that the profile of the curve (d), after milling the $Ta_2O_5 \cdot 3.8H_2O$-derived mixture is very close to that of well-crystallized BMT (curve (e)), implying the electronic state of Ta being already very close to the final product in the mechanically activated precursor.

The difference in the availability of pure-phase BBT and BMT is attributable to the difference in the easiness of bridging bond formation under mechanical stressing. BBT is layered perovskite, in which $(Bi_2O_2)^{2+}$ and $(BaTa_2O_9)^{2-}$ layers line along c axis and Metal (1)-osygen-Metal (2) bridging bonds in BBT perovskite structure are mainly Ta-O-Ba. On the other hand, BMT is complex perovskite in which Ba occupies A site and Mg and Ta occupy B site. In this case, Ta-O-Ba and Ta-O-Mg bonds coexist within a perovskite unit cell. In view of the acid-base reaction across the boundary of solid particles, Ta-O-Ba is easier to form than Ta-O-Mg, because of the higher basicity of Ba than Mg.

5. Ba-Hexaferrites

Z-type hexagonal barium ferrite (Z-hex) is a promising candidate for inductor and electromagnetic wave absorber extending to the GHz region because of its higher resonance frequency and permeability than those of spinel ferrites.[19] However, it is extremely difficult due to its complicated layer structure. From the crystallographic point of view, Z-type ferrite is the most complex in the hexagonal family with its relatives such as M ($BaFe_{12}O_{19}$; M-hex), Y ($Ba_2Co_2Fe_{12}O_{22}$; Y-hex), and W ($BaCo_2Fe_{16}O_{27}$; W-hex)-type ferrites, as shown in Fig. 11. We may regard the Z-hex as a sum of M-hex and Y-hex with its crystalline structure comprising 22 close-packed layers stacked along the hexagonal c-axis.[20]

We have successfully prepared M-hex[21] and Y-hex[22] at considerably low temperatures from the mechanically activated mixtures based on the principle mentioned above. However, we failed to obtain well crystallized, phase pure Z-hex from mechanically activated raw mixtures. We attributed the failure to the preferential formation and high degree of crystallization of M-hex and Y-hex phases, decreasing the potential for the subsequent nuclei-growth processes of Z-hex. In our subsequent trial, we have successfully obtained quasi-phase-pure Z-phase by carefully treating the intermediates.[23] The process is briefly reproduced below.

A stoichiometric mixture for Z-hex composition was milled in water in a conventional rotational ball mill with ZrO_2 balls for 2 h, and dried at 100°C for 12 h, to obtain the starting mixture. We subsequently calcined the starting mixture at 1080°C for 2 h to obtain the intermediate. The intermediate was then dispersed in distilled water and milled with a planetary mill for 1 h The slurry was dried and subsequently calcined for the second time at temperatures between 1180°C and 1230°C for 2 h. The same intermediates were subjected to dry milling for comparison, under the same operational condition.

Fig. 12 exhibits FE-SEM micrographs of the sample preliminarily calcined at 1080°C and subsequently milled for 1 h. We observe agglomerates of submicron sized plate-like

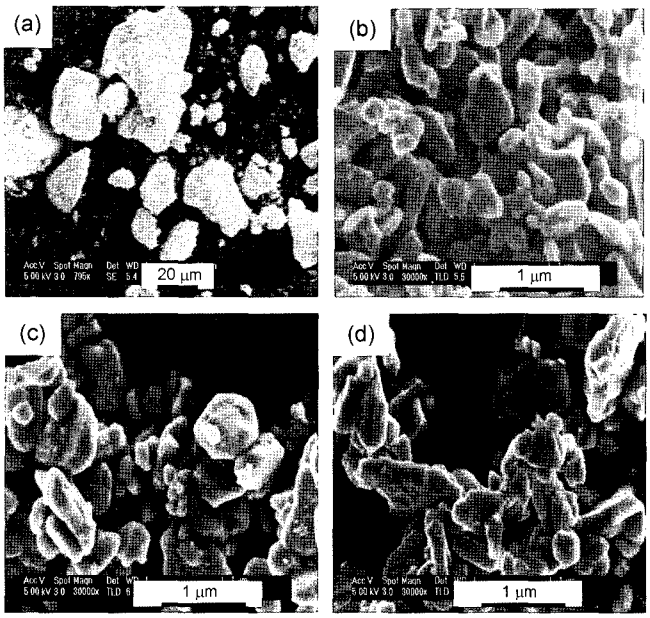

Fig. 12. Field emission scanning electron micrographs of the samples calcined at 1080°C before (a, b -with low and high magnification) and after dry (c) and wet (d) milling for 1 h.

particles. Dry and wet milling of the calcined sample resulted in the agglomerates breakdown, as shown in Fig. 12(c) and 12(d), respectively. The median particle size, d_{50}, determined by a laser diffraction particle size analyzer was, 17.3 μm before milling. The size decreased to 0.15 μm and 0.11 μm by dry and wet milling, respectively.

The calcined sample consists of the M-hex and Y-hex with negligible amounts of barium monoferrite $BaFe_2O_4$ or cobalt spinel $CoFe_2O_4$. Milling little changed the diffraction pattern (not shown, because of similarity) except a little increase in the line width, indicating a decrease in the crystallite size and accumulation of microstrain. The full width at half maximum (FWHM) of the XRD non-overlapping

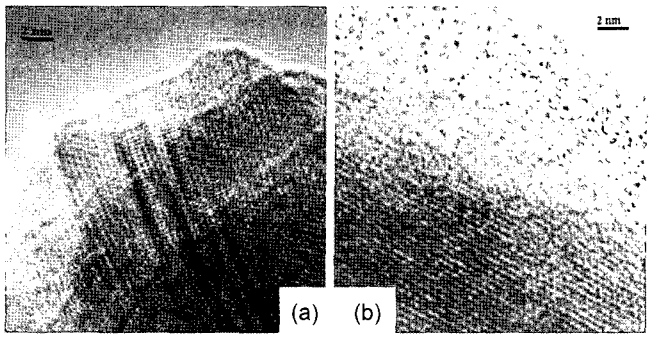

Fig. 13. TEM micrographs of the wet (a) and dry (b) milled samples.

(02$\underline{1}$0) peak of the Y-hex in the calcined intermediate was 0.188° (2θ, CuKα). FWHM increased to 0.282° and 0.235° by dry and wet milling.

Fig. 13 exhibits high-resolution TEM micrographs of the milled samples. In the wet milled sample (Fig. 13(a)), we observe a lattice image without substantial surface amorphization. In contrast, an 8–10 nm thick amorphous layer is recognized on the near surface region of the dry milled sample (Fig. 13(b)).

Fig. 14 shows XRD profiles of the wet and dry milled samples after the second calcination at 1080, 1180, and 1230°C. We observe clear differences between the samples obtained by single and double calcination processes. A raw sample calcined at temperatures below 1180°C contains no Z-hex but only M and Y-hexes. After calcining at 1230°C, Z-hex began to form in a small amount, strong diffraction peaks of the Y-hex phase accompanied by significant coexistence of M-hex. In contrast, wet milling of the intermediates made it possible for Z-phase to crystallize at 1180°C. At 1230°C, Z-hex phase predominates with little Y-hex phase remained.

The relative intensity of the XRD peaks from Z-hex phase differs from those given in the JCPDS card (19-97). The differences are obvious for the peaks at 2θ=23.8°, 30.8°, and

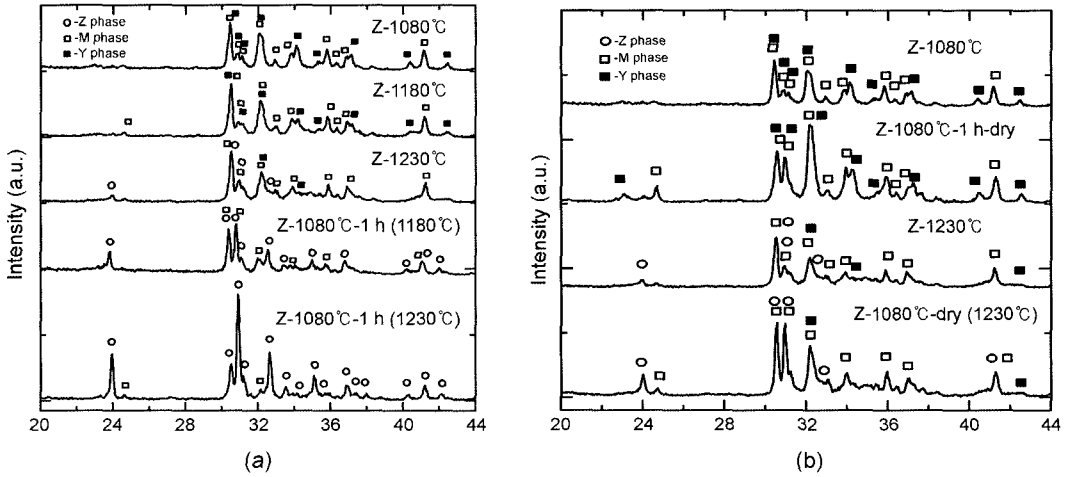

Fig. 14. XRD patterns of the milled samples calcined at different temperatures: (a) wet milled and (b) dry milled.

56.3°, corresponding to (0014), (0018), (0032), respectively. These planes are cleaved out when the particulates of the mixed hexagonal structure are disintegrated. The resulted platelets are oriented preferentially normal to the XRD sample holder, as reported previously.[23] These experimental results demonstrate the favorable effects of wet milling on the intermediates over the dry milling on the Z-hex synthesis.

Z-hex can be regarded as the sum of the layered structure of M-hex and Y-hex as a consequence of the topotactic growth. Moderate milling is therefore essential to preserve the block structures accommodated in the intermediates to make their restacking possible during the second calcinations. Milling the samples significantly decreased the particle size and introduced some structural defects as we recognized from a slight increase in the FWHM. The difference in the Z-hex crystallization behavior between wet and dry milled samples is also related with the structural defects. It is clear that significant surface amorphization by dry milling is unfavorable for the topotaxial formation of Z-hex.

In conclusion, wet milling of the preliminary calcined mixture comprising M-hex and Y-hex phases is beneficial to prepare phase pure Z-hex upon subsequent heating at temperatures as low as 1230°C. Effects of wet milling are disintegration of the agglomerates while preserving the crystalline layer units in favor of their restacking toward Z-hex. Simple dry milling to furnish thick amorphous layer is unfavorable for the synthesis of the phase-pure crystalline states with a complicated layer structure like Z-hex.

6. Concluding Remarks

Importance of the homogeneity of the starting mixture cannot be overemphasized. Homogeneity is diverse from atomic level (10^{-10} m~) to the agglomerates and grains (~10^{-3} m). We have to pay efforts to control so many different factors simultaneously.

For at least two reasons, it is very useful to bridge the dissimilar solid species across the solid boundary to create bridging bonds (HBBs), centered by an oxygen atom. Oxygen-abridged HBBs formed across the solid/solid interface serves as a nucleation site. At the same time, it stabilizes the stoichiometry by bounding even volatile ingredients. Both of these mean the electronic states to become closer to those of products in the reactant mixture prior to calcination.

Increase in the nucleation sites automatically means the decrease in the diffusion path toward the final products. This is obviously assisted by intimate mixing and avoidance of agglomeration. All these are realized simultaneously in a milling pot when we choose appropriate facilities and operational condition.

Finally, the author would like to emphasize the enhancement of the reaction toward the final product. This is only possible through careful analyses of the mixture in the course of entire processes by knowing the reaction mechanisms in detail.

Acknowledgment

The author thanks coauthors of the case studies introduced in the present review, among others Dr. J. G. Baek, Mr. S. Shinohara, Mr. M. Komai, Miss Aoyama, and Miss Kinoshita . This work was partly supported by Grant-in-Aid for the 21st Century COE program "KEIO Life Conjugate Chemistry" from the Ministry of Education, Culture, Sports, Science, and Technology, Japan.

REFERENCES

1. E. Avvakumov, M. Senna, and N. Kosova, "Soft Mechanochemical Synthesis," pp. 145-66, Kluwer Acad. Pub., New York, 2001.
2. M. Senna, "Incipient Chemical Interaction between Fine Particles Under Mechanical Stress-A Feasibility of Producing Advanced Materials via Mechanochemical Routes," *Solid State Ionics*, **3-9** 63-5 (1993).
3. J. F. Liao and M. Senna, "Mechanochemical Dehydration and Amorphization of Hydroxides of Ca, Mg, and Al on Grinding with and Without SiO_2," *Solid State Ionics*, **66** 313-19 (1993).
4. T. Watanabe, T. Isobe, and M. Senna, "Mechanisms of Incipient Chemical Reaction between $Ca(OH)_2$ and SiO_2 Under Moderate Mechanical Stressing, II. Examination of a Radical Mechanism by an EPR Study," *J. Solid State Chem.*, **122** 291-96 (1996).
5. T. Watanabe, T. Isobe, and M. Senna, "Mechanisms of Incipient Chemical Reaction between $Ca(OH)_2$ and SiO_2 Under Moderate Mechanical Stressing, III. Changes in the Short Range Ordering through the Mechanical and Thermal Processes," *J. Solid State Chem.*, **130** 284-89 (1997).
6. M. Senna, "Mild Mechanical Stressing on Mixtures to a Precursor for Homogeneous Complex Oxides," *Chem. Rev.*, **123** 263-84 (1998).
7. M. Senna, "Recent Development of Materials Design through a Mechanochemical Route," *Int. J. Inorg. Mater.*, **3** 509-14 (2001).
8. M. Senna, "Charge Transfer and Hetero-Bonding Across the Solid-Solid Interface at Room Temperature," *Mater. Sci. Eng. A*, **A304-306** 39-44 (2001).
9. Y, Fujiwara, T. Isobe, M. Senna, and J. Tanaka, "Effects of Reduced Coordination Number for Ca on the Electron Redistribution During Ca-O-Si Bridge Bonding from CaO or $Ca(OH)_2$ and SiO_2," *J. Phys. Chem.*, **103** 9842-46 (1999).
10. M. Senna, Y. Fujiwara, T. Isobe, and J. Tanaka, "Molecular Dynamic-Molecular Orbital Combined Study on the Solid State Interfacial Reaction Under Mechanical Stressing," *Solid State Ionics*, **141-142** 31-8 (2001).
11. J. G. Beak, T. Isobe, and M. Senna, "A New Fabrication Technique for Perovskite $0.9Pb(Mg_{1/3}Nb_{2/3})O_3$. $0.1TiO_2$ Ceramics via a Soft-Mechanochemical Route", *J. Am. Ceram. Soc.*, **80** 973-81 (1997).
12. K. Hamada, S. Yamamoto, M. Nagano, and M. Senna,

"Measurement of Compressive and Shear Forces in Multiring Media Mill," *J. Chem. Eng. Jpn.*, **30** 756-59 (1997).
13. S. Shinohara, T. Isobe, and M. Senna, "Synthesis of Phase Pure $Pb(Zn_xMg_{1-x})$-$Nb_{2/3}O_3$ up to x=0.7 from a Single Mixture via a Soft-Mechanochemical Route," *J. Am. Ceram. Soc.*, **83** 3208-10 (2000).
14. N. Wakiya, N. Isizawa, and N. Mizutani, "Thermal Stability of $Pb(Zn_{1/3}Nb_{2/3})O_3$ (PZN) and Consideration of Stabilization Conditions of Perovskite Type Compounds," *Mater. Res. Bull.*, **30** 1121-31 (1995).
15. N. Wakiya and Masters Thesis, "Crystallographical Analysis of Lead Containing Perovskites," *Tokyo Inst. Technol.*, 1995.
16. H. M. Jang, S. R. Cho, and K. M. Lee, "Mechanism of Formation of Perovskite Phase and Dielectric Properties of $Pb(Zn,Mg)_{1/3}Nb_{2/3}O_3$ Ceramics Prepared by Columbite Precursor Routes," *J. Am. Ceram. Soc*, **78** 297-304 (1995).
17. Y. Fang, A. Hu, Y. Gu, and Y. J. Oh, "Synthesis of $Ba(Mg_{1/3}Ta_{2/3})O_3$ Microwave Dielectrics by Solid State Processing," *J. Eur. Ceram. Soc.*, **23** 2497-502 (2003).
18. J. Y. Wu and X. M. Chen, "Microwave Dielectric Characteristics of $Ba(Mg_{1/3}Ta_{2/3})O_3$ Ceramics Sintered at Low-Temperatures," *Mater Sci. Eng.*, **B100** 244-49 (2003).
19. O. Sakaguchi, T. Kagotani, D. Book, H. Nakamura, S. Sugimoto, M. Okada, and M. Homma, "Synthesis and Magnetic Properties of Ferroxplana Type Ferrite," *Mater. Trans. JIM*, **37** 878-82 (1996).
20. H. A. Elkady, M. M. Abou-Sekkina, and K. Nagorny, "New Information on Mössbauer and Phase Transition Properties of Z-Type Hexaferrites," *Hyperfine Interactions*, **128** 423-32 (2000).
21. J. Temuujin, M. Aoyama, M. Senna, T. Masuko, C. Ando, and H. Kishi, "Crystallization of M-Type Hexagonal Ferrites from Mechanically Activated Mixtures of Barium Carbonate and Goethite," *Mater. Res. Bull.*, in press.
22. J. Temuujin, M. Aoyama, M. Senna, T. Masuko, C. Ando, and H. Kishi, "Synthesis of Y-Type Hexaferrites via a Soft Mechanochemical Route", *J. Solid State Chem.*, **177** 3903-08 (2004).
23. J. Temuujin, M. Aoyama, M. Senna, T. Masuko, C. Ando, and H. Kishi, "Benefits of Mild Wet Milling of the Intermediates for the Synthesis of Phase-Pure Z-Type Hexaferrite," *J. Mater. Res.*, **20** 1939-42 (2005).